

Soft Matter

Accepted Manuscript

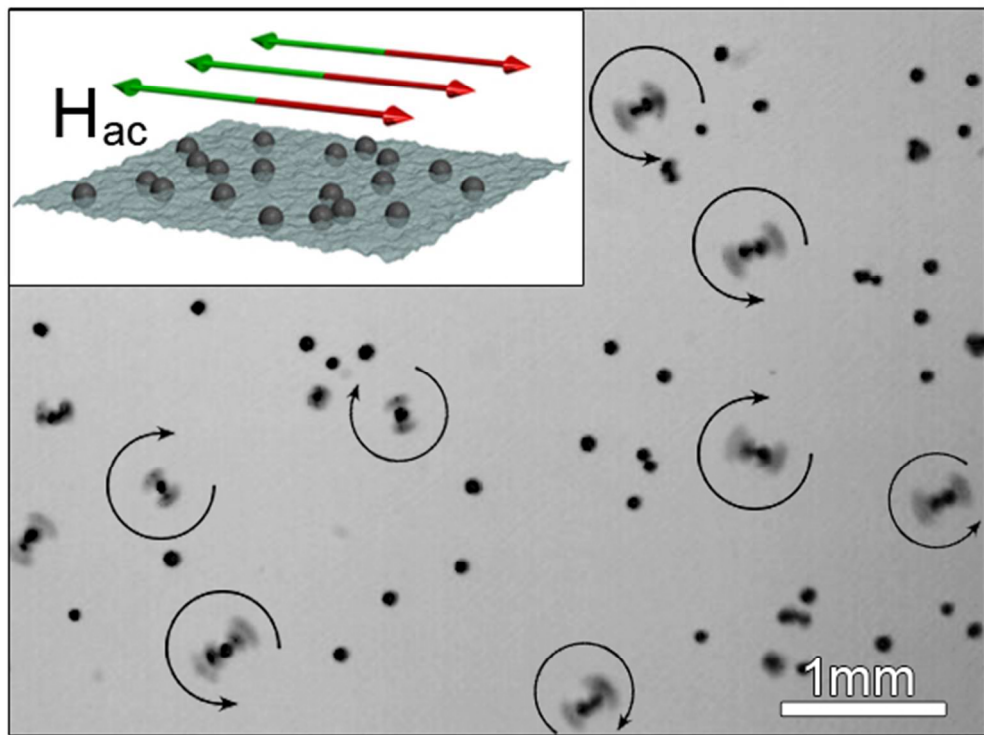


This is an Accepted Manuscript, which has been through the Royal Society of Chemistry peer review process and has been accepted for publication.

Accepted Manuscripts are published online shortly after acceptance, before technical editing, formatting and proof reading. Using this free service, authors can make their results available to the community, in citable form, before we publish the edited article. We will replace this Accepted Manuscript with the edited and formatted Advance Article as soon as it is available.

You can find more information about Accepted Manuscripts in the [Information for Authors](#).

Please note that technical editing may introduce minor changes to the text and/or graphics, which may alter content. The journal's standard [Terms & Conditions](#) and the [Ethical guidelines](#) still apply. In no event shall the Royal Society of Chemistry be held responsible for any errors or omissions in this Accepted Manuscript or any consequences arising from the use of any information it contains.



Velocity statistics of strongly coupled dynamic micro-rotors in out-of-equilibrium magnetic suspensions
215x164mm (72 x 72 DPI)

Velocity statistics of dynamic spinners in out-of-equilibrium magnetic suspensions[†]

Alexey Snezhko,^{*a} and Igor S. Aranson^a

Received Xth XXXXXXXXXX 2014, Accepted Xth XXXXXXXXXX 20XX

First published on the web Xth XXXXXXXXXX 200X

DOI: 10.1039/b000000x

We report on the velocity statistics of an out-of-equilibrium magnetic suspension in a spinner phase confined at a liquid interface. The suspension is energized by a uniaxial alternating magnetic field applied parallel to the interface. In a certain range of the magnetic field parameters the system spontaneously undergoes a transition into a dynamic spinner phase (ensemble of hydrodynamically coupled magnetic micro-rotors) comprised of two subsystems: self-assembled spinning chains and a gas of rotating single particles. Both subsystems coexist in a dynamic equilibrium via continuous exchange of the particles. Spinners excite surface flows that significantly increase particle velocity correlations in the system. For both subsystems the velocity distributions are strongly non-Maxwellian with nearly exponential high-energy tails, $P(v) \sim \exp(-|v/v_0|)$. The kurtosis, the measure of the deviation from the Gaussian statistics, is influenced by the frequency of the external magnetic field. We show that in the single-particle gas the dissipation is mostly collisional, whereas the viscous damping dominates over collisional dissipation for the self-assembled spinners. The dissipation increases with the frequency of the applied magnetic field. Our results provide insights into non-trivial dissipation mechanisms determining self-assembly processes in out-of-equilibrium magnetic suspensions.

1 Introduction

Understanding fundamental mechanisms determining the behavior of out-of-equilibrium colloidal systems is an important prerequisite for the discovery of new self-assembled materials and structures at micro and nano-scales. Out-of-equilibrium self-assembly holds a promise for a design strategy of complex materials not generally available near thermodynamic equilibrium^{1–12}.

A series of experiments on granular gases driven mechanically^{13–20} or electrostatically^{21,22} and numerical simulations^{20,23–27} demonstrated that even dilute systems of macroscopic particles behave differently than molecular gases at equilibrium. Due to the inelasticity of particle interactions, the velocity distributions significantly deviate from the Maxwellian velocity distribution. In particular, the high-energy tails of the velocity distribution become stretched-exponential, $P(v) \sim \exp(-|v/v_0|^\xi)$, where $v_0 = \langle v^2 \rangle^{1/2}$ is the root mean squared (r.m.s.) velocity. The exponent $\xi = 3/2$, expected from a kinetic theory for inelastic spheres with hard-core repulsion, was indeed observed in a set of experiments with vigorously shaken grains^{14,28}. However, in the majority of systems the interactions between particles are not reduced

to simple inelastic collisions with hard-core repulsion. Viscous damping and long range magnetic interactions lead to nearly exponential high-energy tails with $\xi \approx 1$ in the system of electrostatically driven magnetic grains²². For dense granular systems, the build-up of the velocity correlations with the increase in the particle packing fraction led to a significant deviation from the previously reported stretched-exponential behavior with $\xi = 3/2$ ¹⁹. The deviation was shown to be proportional to the number of particles in the system. It was also demonstrated theoretically that under an extreme driving condition (the injection rate much smaller than the collision rate), the high energy tail of the velocity distribution shows a power-law behavior²⁹.

In this paper we focus on particle velocity statistics in an out-of-equilibrium suspension of ferromagnetic particles at a liquid-air interface. The suspension is driven away from equilibrium by a uniaxial alternating magnetic field applied parallel to the interface. The system demonstrates a variety of nontrivial dynamic self-assembled states³⁰ in a wide range of the magnetic field parameters. Here we focus on a spinner phase (strongly coupled micro-rotors) where dynamically assembled short spinning chains coexist with the gas of rotating single particles. In a steady state spinners (chains with at least 2 particles) and the gas are at a dynamic equilibrium and continuously exchange particles. However, particle interactions within each subsystem happen to be very different. We carry out a set of experiments at different frequencies of the ap-

[†] Electronic Supplementary Information available. See DOI: 10.1039/b000000x/

^a Materials Science Division, Argonne National Laboratory, 9700 S. Cass Avenue, Argonne, IL 60439, USA. E-mail: snezhko@anl.gov

plied magnetic field within the boundary of the spinner phase, and investigate how the particle interactions affect the velocity statistics. Due to mechanism of forcing involved (alternating magnetic field) and geometry of the experiment (in-plane forcing) there are no out-of-plane components of the velocities. We find that the velocity distributions for spinners and gas subsystems are distinctively different and strongly non-Maxwellian, with nearly exponential high-energy tails. Our results indicate that the velocity statistics of hydrodynamically coupled magnetic spinners can be tuned *in situ* by the parameters of the driving field.

2 Experimental details

In our experiments ferromagnetically ordered nickel spheres with an average radius of $45\mu\text{m}$ ($40 - 50\mu\text{m}$ uniform size distribution) are dispersed at a water-air interface and supported by a surface tension in a 5cm round glass container. The container is placed inside a pair of precision Helmholtz coils. The coils create an alternating magnetic fields along the liquid-air interface. The suspension was energized by an alternating magnetic field, $H_x^{ac}(t) = H_0 \sin(2\pi ft)$, see inset to Fig. 1a for the schematics of the experiment. The suspension was maintained in a spinner phase (see Ref.³⁰ for details of other phases). The amplitude of the magnetic field H_0 was in the range of $27 - 31$ Oe and the frequency f was in the range of $35 - 120$ Hz. All results on the velocity statistics reported here were obtained at a fixed low surface coverage $\phi \simeq 1.6\%$ (high surface coverages produce different dynamic phases³¹) and fixed field amplitude $H_0 = 30.4$ Oe. The x axis was chosen to be along the driving field direction. Dynamics of particles is monitored by a high-speed CCD camera mounted on a microscope stage. We recorded image sequences (1280x1024 resolution) at a frame rate of 400fps. Image and data analysis of the time sequences were carried out using MatPIV, ImageJ and custom scripts.

The majority of experiments on velocity distributions in driven granular/colloidal systems relied on the energy injection from the walls of the container (mechanical shaking^{13–20}, electrostatic charging from the walls^{21,22}, etc.) and provided access to a quasi-2d velocity statistics. In our experiment, however, the excitation mechanism is significantly different. We use an alternating magnetic field to drive the system out of equilibrium. Upon application of the magnetic field, all particles are forced to respond the same way regardless of their position or orientation with respect to the container walls. Ferromagnetic particles have to align their magnetic moments with the instant orientation of the applied magnetic field. Due to a strong pinning of the magnetic moment inside each particle, the reorientation proceeds predominantly through mechanical rotation of particles rather than rotation of the moment inside the particle^{32,33}. Alternating magnetic field forcing along the

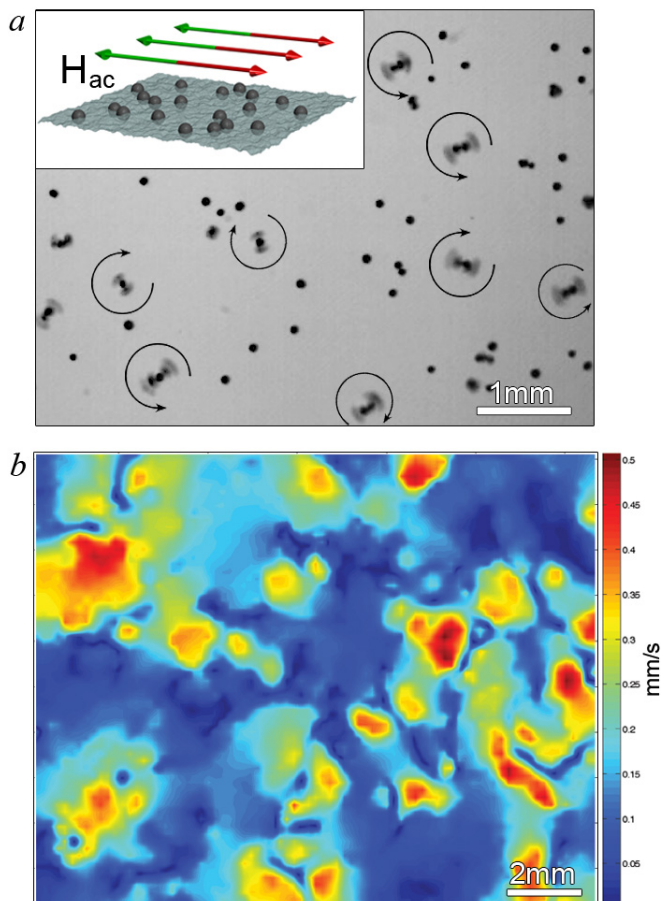


Fig. 1 Spinner phase. (a) Snapshot of a spinner phase created at $f = 60$ Hz, $H_0 = 30.4$ Oe of the in-plane alternating magnetic field. One sees individual particles as well as short self-assembled spinning chains of particles. The image exposure time was intentionally set to a high value to visualize the blurring of chains due to fast rotation. Arrows around the spinners show the rotation direction of a randomly selected spinner. *Inset:* Schematics of the experiment. A uniaxial alternating magnetic field is applied parallel to the water-air interface. (b) A snapshot of a typical hydrodynamic surface flow distribution generated by a spinner phase ($f = 70$ Hz, $H_0 = 28$ Oe) at the interface.

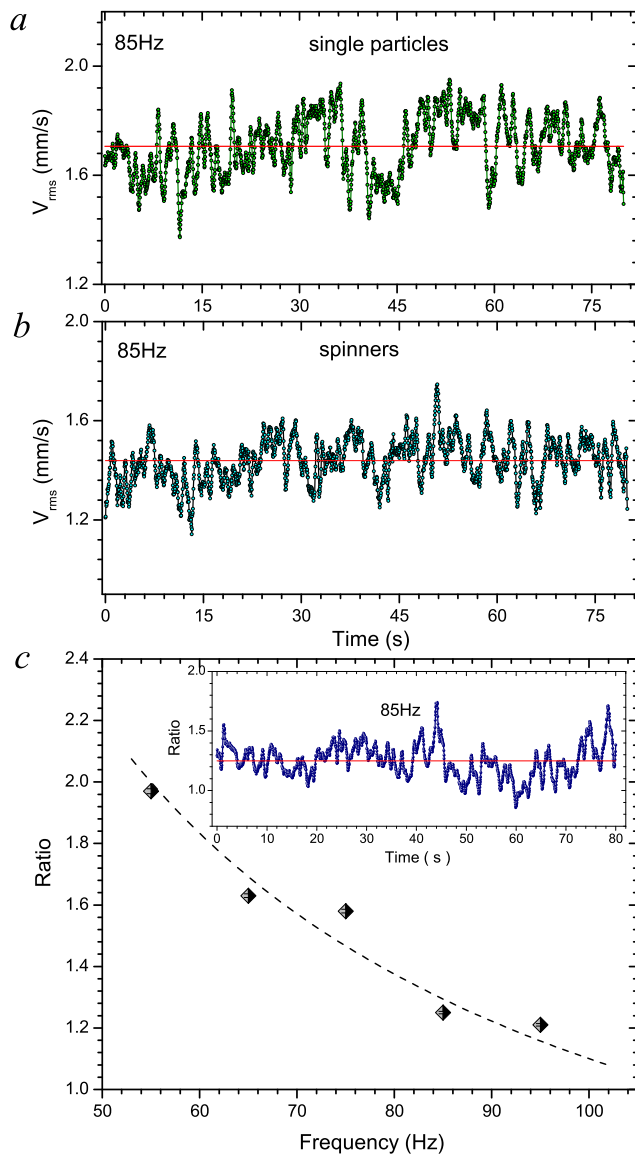


Fig. 2 Root mean square (r.m.s.) velocity (V_{rms}) of single particles (a) and spinners (b) as a function of time. The dynamic spinner phase was generated at $f = 85$ Hz, $H_0 = 30$ Oe applied magnetic field. Solid line is an average r.m.s. velocity of the corresponding subsystem. (c) Frequency dependence of the ratio between the number of single particles and spinners. *Inset:* The ratio as a function of time at $f = 85$ Hz, $H_0 = 30$ Oe.

liquid interface transfers torques rather than forces and enables access to velocity statistics with no out-of-plane components of the particles velocities. Particles' rotations create local interface deformations and hydrodynamic surface flows. In turn the flows alter particle interaction profiles. The local magnetic order in suspension at equilibrium is governed by dipole-dipole interactions between particles that naturally favor a formation of head-to-tail chains. In contrast, the outcome of dynamic self-assembly in an alternating magnetic field is often nontrivial^{8,34–39}. An intricate balance between magnetic and hydrodynamic interactions gives rise to an unexpected spinner phase in the system under study, see Fig. 1. The phase is characterized by a well defined spinner's length and a ratio between total number of rotating chains and single particles. Furthermore, the ratio is controlled by the parameters of the driving magnetic field³⁰. The system is dynamic by nature: spinners and particles vigorously move over the interface, collide, disintegrate and reassemble (see supplementary Video 1 illustrating overall appearance of the spinner phase and Video 2 showing detailed dynamics). Correspondingly, self-induced surface hydrodynamic flows evolve in a seemingly random manner, see Fig. 1b and supplementary Video 3. This flow velocity field was visualized by means of particle image velocimetry (PIV) of the tracer particles ($10 - 15 \mu\text{m}$ copper spheres) dispersed at the interface.

3 Results and discussions

To characterize the dynamic states at different frequencies of the applied magnetic field, we measured the *r.m.s.* velocities for the spinner and single particle subsystems individually. While the instantaneous values of the *r.m.s.* velocities fluctuate as shown in Fig. 2a,b, their time averaged values provide an adequate description of the system state as a function of the applied magnetic field parameters. The ratio between the number of single particles and spinners is also sensitive to the parameters of the magnetic field. Due to vigorous self-induced surface flows and long-range magnetic dipole interactions, single particles and spinners are continuously involved in interactions. Instantaneous ratio between number of elements in the subsystem (either single particles or chains) fluctuates, see inset to Fig. 2c. However, the time averaged ratio exhibits a well-defined trend, see Fig. 2c. As the frequency of the alternating field increases, the ratio decreases and reaches almost one-to-one ratio at the frequencies above 100 Hz. While the spinner size decreases with the frequency of the driving field³⁰ the overall number of spinners increases. The characteristic *r.m.s.* velocity of the spinners does not exhibit monotonic behavior and fluctuates within 14% with the excitation frequency. Above 120 Hz, a transition into a different (wires) dynamic phase occurs³⁰, that is not a focus of the present study.

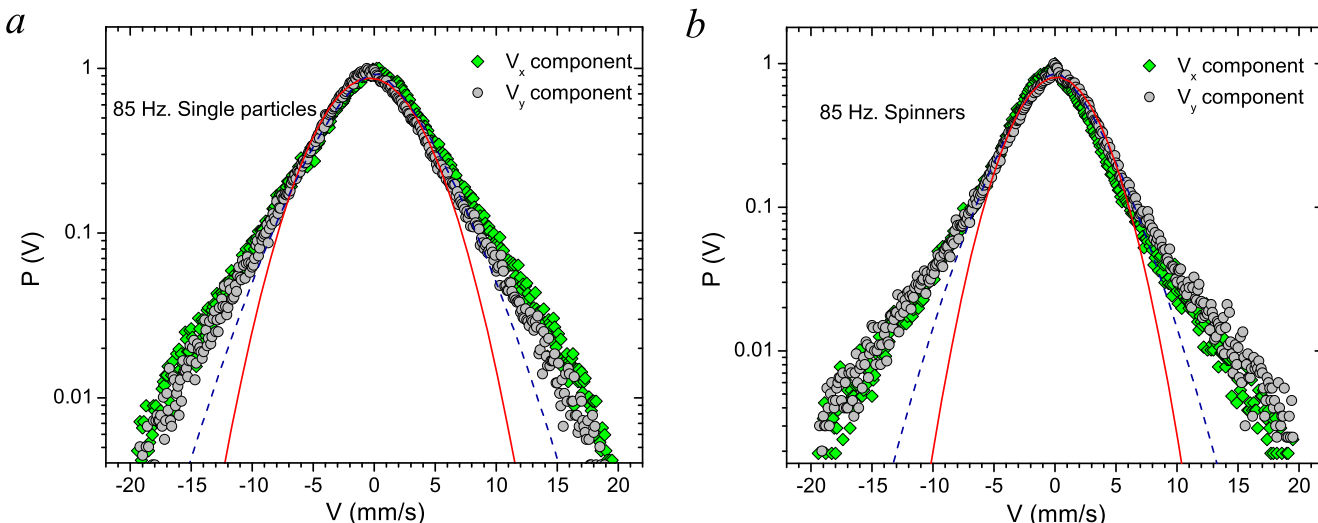


Fig. 4 Representative distributions for v_x and v_y velocity components for single particles (a) and spinners (b). Displayed results correspond to $f = 30$ Oe, $H_0 = 85$ Hz. Solid lines depict the Maxwellian distributions; dashed curves show a stretched exponential distribution with $\xi = 3/2$.

To characterize the self-generated surface hydrodynamic flows, we calculate a flow velocity spatial correlation function,

$$C_{space}(s) = \frac{\langle \vec{v}(r)\vec{v}(r+s) \rangle_r - \langle \vec{v}(r) \rangle_r^2}{\langle v^2(r) \rangle_r - \langle \vec{v}(r) \rangle_r^2}$$

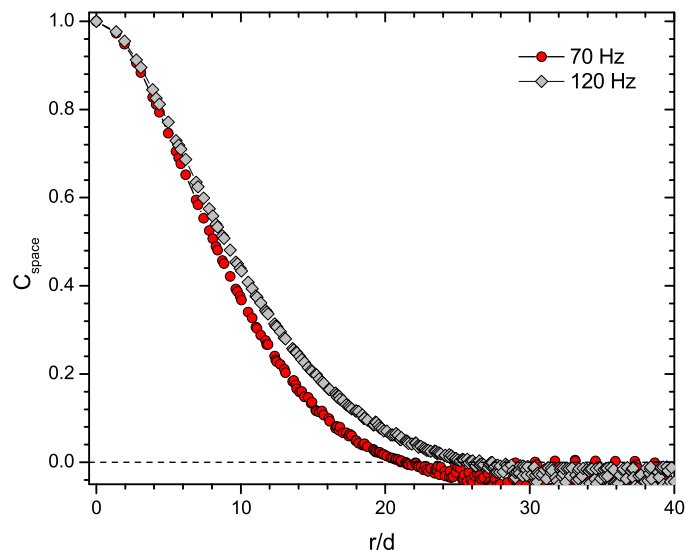


Fig. 3 Velocity spatial correlation function of the self-induced surface hydrodynamic flows in a spinner phase. Distance is normalized by the particle diameter d .

The results shown in Fig. 3 reveal a long-range spatial correlations of the flows (of the order of 15-20 particle diameters). The correlation length exhibits almost no dependence on the frequency f . Such a large correlation length in the spinner phase suggests that long-range hydrodynamic interactions should dominate short-range magnetic dipole-dipole interactions.

Both v_x and v_y particle velocity components along the interface can be accessed by the means of a high-speed video microscopy and particle tracking. Representative results for spinner and single particle subsystems are shown in Fig. 4. Strikingly, even though the applied magnetic field is uniaxial and aligned along the x -axis, the system exhibits practically an isotropic spatial particle distribution and isotropic velocity distributions (velocity distributions for both v_x and v_y components coincide). That observation indicates that the large-scale dynamics in the spinner phase is solely defined by the interaction profiles of the particles, and apparent anisotropy of the driving is averaged out by the system response.

For both single particle and spinner subsystems the velocity distributions are clearly non-Maxwellian. The distribution tails are significantly overpopulated compared to the Gaussian distributions (shown as solid red curves) expected for non-dissipative gases at equilibrium. The stretched exponential distribution with the exponent $\xi = 3/2$ observed for dissipative granular gases with hard-core repulsion (shown as dashed curves in Fig. 4) also does not provide a good description of

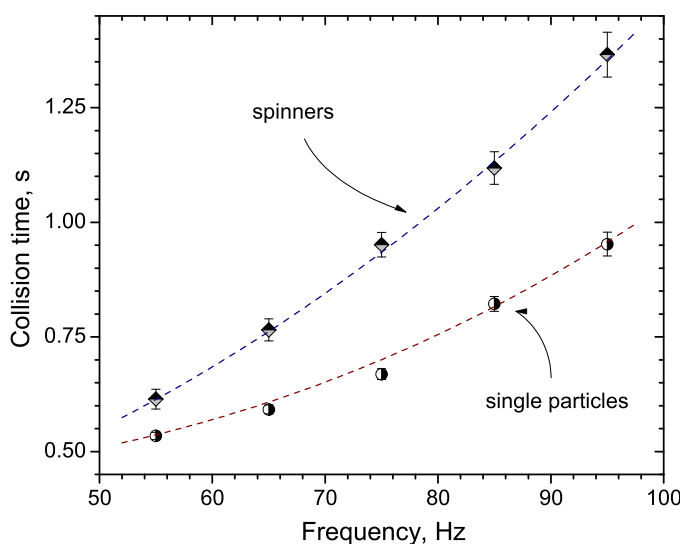


Fig. 5 Collision time as a function of the magnetic field frequency f for spinners (diamonds) and single particles (circles). Amplitude of the alternating magnetic field was set to $H_0 = 30$ Oe. The dashed lines are guides to the eye.

the data. To obtain insights into the origin of the apparent differences in the resulting velocity distributions for single particles and spinners, we analyzed typical collision times in those subsystems. The collision time is determined as a mean lifetime of a particle's (or spinner's) trajectories before any collision occurs. The same analysis was performed at different frequencies of the magnetic field within the spinner phase region. The results of the analysis are shown in Fig. 5.

For both subsystems the collision times demonstrate a strong dependence on the frequency of the magnetic field. The stronger dependence for the spinners (the collision time more than doubles in a 40Hz window) reflects the fact that a spinner creates a much stronger vortical flow than a single particle due to their shape and size differences. Resulting flow acts as a “protective bumper” by diverting incoming particles (due to the centrifugal force exerted on the particle by a vortical flow). Since the magnitude of the flow generated by a spinner increases with the frequency, the depletion zone around the spinner grows with the frequency as well. The fact that the collision time for single particles substantially smaller than that for spinners suggests that the collisional dissipation for the single particles subsystem plays a bigger role than for the spinner subsystem.

To quantify the deviations of the obtained velocity distribution from the Gaussian law we calculated the kurtosis of the distributions in a range of frequencies within the boundaries of the spinner phase. Kurtosis is defined as follows, $k = \frac{\langle v^4 \rangle}{\langle v^2 \rangle^2}$ and characterizes a flatness (or peakedness) of a distribution.

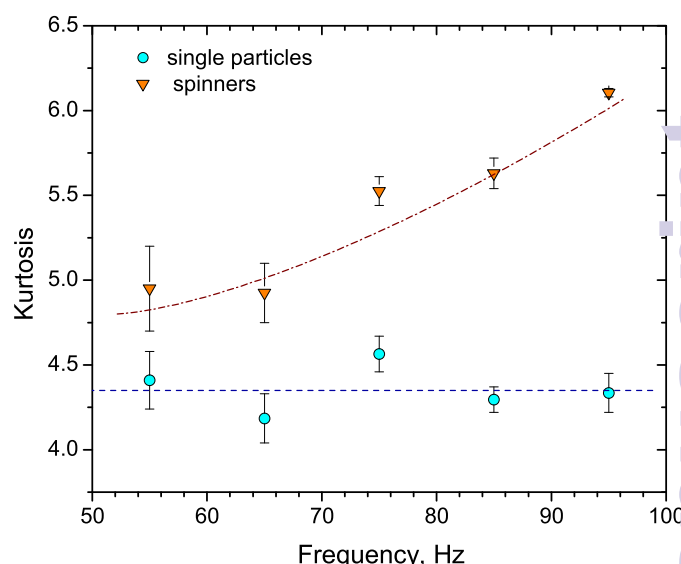


Fig. 6 Kurtosis of velocity distributions for spinners (triangles) and single particles (circles) as a function of the magnetic field frequency f . Amplitude of the magnetic field H_0 was fixed at 30 Oe. The dashed lines are guides to the eye.

For pure Gaussian distributions $k = 3$. For stretched exponential distributions with $\xi = 3/2$ the kurtosis is $k \simeq 3.76$. For systems with predominantly viscous dissipation, the velocity distribution is almost exponential^{20,22} with the kurtosis $k = 6$. For dominant magnetic interactions there is an excellent agreement between the experiment and theory (thermally forced Maxwell molecules⁴⁰) suggesting kurtosis $k \simeq 3.55$ ²². In the later case even though the tails of the distribution are close to simple exponential ones, its core remains approximately Maxwellian³². Analysis of the kurtosis associated with the velocity distributions provides an important clues on the dominant forces underlying the complex dynamics of out-of-equilibrium system and how they change in response to parameters of the external forcing.

We performed a set of experiments at different frequencies of the magnetic field covering the entire range of the spinner phase. Velocity distributions and the kurtosis for single particles and spinners have been extracted from the data. The results are shown in Fig. 6.

Single particles and spinners demonstrate notably different kurtosis of their distributions implying a significant difference in the dominant mechanism of the energy dissipation in these two subsystems. Furthermore, the frequency dependence of the kurtosis for both subsystems is strikingly different. As for the single particles, the effect of the frequency on the kurtosis is negligible: the kurtosis does not change in the entire frequency range keeping its value at $k \simeq 4.4$. In contrast, the kurtosis for the spinner distributions is strongly influenced by the

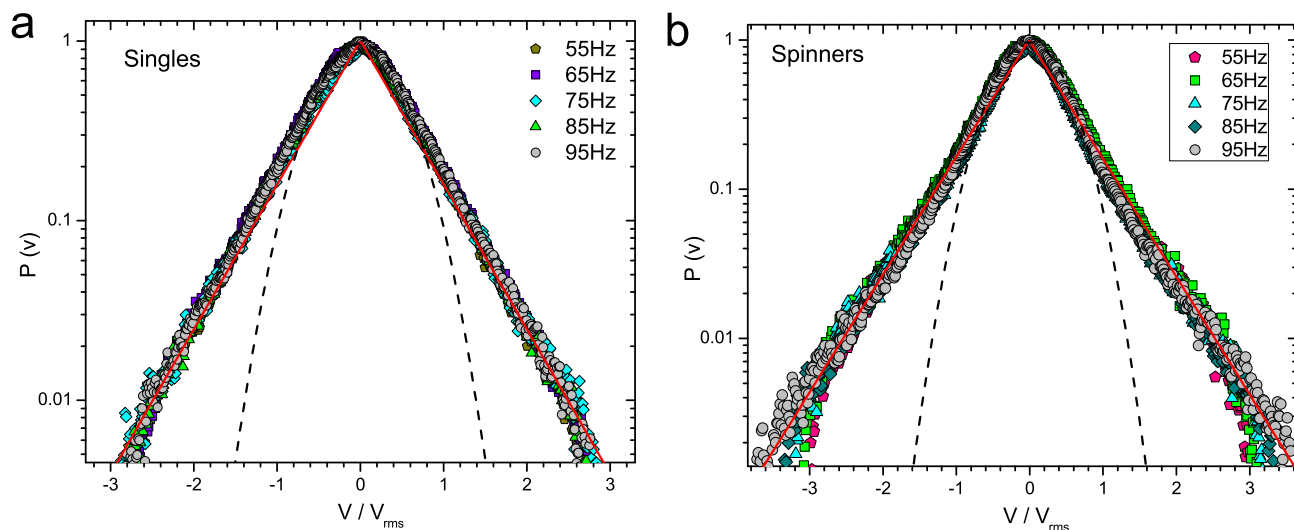


Fig. 7 Velocity distributions for single particles (a) and spinners (b) at different frequencies within the spinner phase. Each distribution is normalized to be unity at its maximum. Velocity is normalized by the corresponding v_{rms} values. Solid lines are pure exponential distributions $P(v) \sim \exp(-|v/v_{rms}|)$. Dashed curves are the Maxwellian distributions. All distributions have approximate Maxwellian cores. A crossover to exponential behavior occurs for $|v| > v_{rms}$.

frequency of the driving magnetic field. It grows from $k \simeq 4.8$ at the low frequency boundary to $k \simeq 6$ at the top boundary (see Fig. 6).

For both subsystems there are two apparent dominant dissipation mechanisms: collisional (due to inelastic collisions with steric repulsions) and viscous drag. The single particle subsystem of the out-of-equilibrium suspension exhibits the kurtosis values that are much closer to the value of $k = 3.6$. This observation indicates a dominance of short-range inelastic collisions⁴⁰. In the case of spinners the kurtosis values on the other hand are closer to a pure exponential value of $k = 6$ suggesting that viscous damping is a key dissipation mechanism for the self-assembled spinners. As the frequency of the magnetic field increases, the collisional dissipation for spinners becomes even less important (likely due to the formation of a “protective bumpers” around rapidly rotating spinners) and the kurtosis reaches $k \simeq 6$ at the high frequency boundary of the spinner phase (see Fig. 6).

For the sake of comparison, we plot in Fig. 7 a set of normalized velocity distributions obtained in the range of frequencies within the spinner phase region. The velocity components are scaled by corresponding v_{rms} values. In both cases (single particles and spinners) the distributions predominantly coincide. However, in the case of spinners one can clearly distinguish a tendency of the high-velocity tails to change gradually their slopes with the frequency of the magnetic field

(Fig. 6b). In contrast, velocity distributions for single particles do not follow this trend and sit on top of each other for all frequencies. This effect has been already captured by the kurtosis analysis and manifests the stronger influence of the viscous damping in the spinner subsystem. For both subsystems, the core of distributions remain approximately Maxwellian (dashed curves in Fig. 7a,b) even though the high-velocity tails of the distributions are close to simple exponential. These results are in contrast with almost exponential distribution observed for non-magnetic granular gases in liquids²². Conversely, similar Maxwellian cores were previously observed in dry granular gases with strong magnetic dipole-dipole interactions²².

4 Conclusions

Out-of-equilibrium magnetic suspensions confined at a liquid interface and energized by an external uniaxial alternating magnetic field exhibit unexpectedly complex collective dynamics. Under certain conditions controlled by the parameters of the magnetic field, the suspension spontaneously breaks the symmetry of the applied uniaxial field and new dynamic spinner phase emerges. In this phase a fraction of the particles dynamically self-assemble into short chains (spinners), rotating with the frequency of the applied field in either direction. The spinners and remaining rotating single particles

are in a dynamic equilibrium by assembly/disassembly and collision processes. Viscous torques created by the spinners trigger strong long-range surface flows at the interface. Both, single particles and spinners, are advected by the self generated flows. The surface flows contribute to significant spatial velocity correlations observed between the particles.

Both subsystems, i.e. spinners and single particles, exhibit non-Maxwellian velocity distributions. High-energy tails of the distributions are overpopulated and described by an almost exponential law. Analysis of the kurtosis associated with the velocity distributions revealed two distinctively different dominant mechanisms controlling out-of-equilibrium dynamics of hydrodynamically coupled rotators in a magnetic suspension. We demonstrate that for the self-assembled spinners the viscous damping dominates over collisional dissipation and increases with the frequency of the magnetic field. In contrast, a gas of single particles exhibits velocity distributions unaffected by the magnetic field frequencies. Our experiments suggest that velocity distributions in out-of-equilibrium magnetic suspensions are not universal and depend on the mechanism of the dissipation, and could be strongly influenced by the parameters of the energizing fields.

Our results provide insights into non-trivial mechanisms controlling self-assembly in out-of-equilibrium systems. Careful analysis of the statistical properties of distinct dynamic phases helps identifying dominant dissipation mechanisms, e.g. short-range collisions vs viscous drag. These results can be used, for example, in continuous coarse-grained description of out-of-equilibrium suspensions. Observation of spinner phase in the bulk of the fluid is another interesting extension of our work. This phase can be efficiently used, for example, for bulk mixing.

5 Acknowledgements

The research was supported by the U.S. DOE, Office of Basic Energy Sciences, Division of Materials Science and Engineering under the Contract No. DE AC02-06CH11357.

References

- 1 G. Whitesides and B. Grzybowski, *Science*, 2002, **295**, 2418–2421.
- 2 A. Demortiere, A. Snezhko, M. V. Sapozhnikov, N. Becker, T. Proslier and I. S. Aranson, *Nature Communications*, 2014, **5**, 3117.
- 3 J. E. Martin, E. Venturini, G. L. Gulley and J. Williamson, *Phys. Rev. E*, 2004, **69**, 021508.
- 4 M. E. Leunissen, H. R. Vutukuri and A. van Blaaderen, *Adv. Mater.*, 2009, **21**, 0935–9648.
- 5 J. E. Martin and A. Snezhko, *Reports on Progress in Physics*, 2013, **76**, 126601.
- 6 N. Osterman, I. Poberaj, J. Dobnikar, D. Frenkel, P. Ziherl and D. Babić, *Phys. Rev. Lett.*, 2009, **103**, 228301.
- 7 S. Gangwal, A. Pawar, I. Kretzschmar and O. D. Velev, *Soft Matter*, 2010, **6**, 1413–1418.
- 8 R. Alert, J. Casademunt and P. Tierno, *Phys. Rev. Lett.*, 2014, **113**, 198301.
- 9 D. H. Read and J. E. Martin, *Advanced Functional Materials*, 2010, **20**, 1577–1584.
- 10 S. K. Smoukov, S. Gangwal, M. Marquez and O. D. Velev, *Soft Matter*, 2009, **5**, 1285–1292.
- 11 I. S. Aranson, *Physics-Uspekhi*, 2013, **56**, 79.
- 12 I. S. Aranson, *Comptes Rendus Physique*, 2013, **14**, 518–527.
- 13 W. Losert, D. Cooper, J. Delour, A. Kudrolli and J. Gollub, *Chaos*, 1999, **9**, 682–690.
- 14 F. Rouyer and N. Menon, *Phys. Rev. Lett.*, 2000, **85**, 3676–3679.
- 15 D. Blair and A. Kudrolli, *Phys. Rev. E*, 2003, **67**, 041301.
- 16 J. Olafsen and J. Urbach, *Phys. Rev. Lett.*, 1998, **81**, 4369–4372.
- 17 A. Kudrolli, M. Wolpert and J. Gollub, *Phys. Rev. Lett.*, 1997, **78**, 1383–1386.
- 18 J. Olafsen and J. Urbach, *Phys. Rev. E*, 1999, **60**, R2468–R2471.
- 19 D. Blair and A. Kudrolli, *Phys. Rev. E*, 2001, **64**, 050301.
- 20 J. van Zon, J. Kreft, D. Goldman, D. Miracle, J. Swift and H. Swinney, *Phys. Rev. E*, 2004, **70**, 040301.
- 21 I. Aranson and J. Olafsen, *Phys. Rev. E*, 2002, **66**, 061302.
- 22 K. Kohlstedt, A. Snezhko, M. Sapozhnikov, I. Aranson, J. Olafsen and E. Ben-Naim, *Phys. Rev. Lett.*, 2005, **95**, 068001.
- 23 E. Grossman, T. Zhou and E. BenNaim, *Phys. Rev. E*, 1997, **55**, 4200–4206.
- 24 S. Moon, M. Shattuck and J. Swift, *Phys. Rev. E*, 2001, **64**, 031303.
- 25 R. Soto, J. Piasecki and M. Mareschal, *Phys. Rev. E*, 2001, **64**, 031306.
- 26 J. Brey and M. Ruiz-Montero, *Phys. Rev. E*, 2003, **67**, 021307.
- 27 V. V. Prasad, S. Sabhapandit and A. Dhar, *EPL*, 2013, **104**, 54003.
- 28 T. Van Noije and M. Ernst, *Granular Matter*, 1998, **1**, 57–64.
- 29 W. Kang, J. Machta and E. Ben-Naim, *EPL (Europhysics Letters)*, 2010, **91**, 34002.
- 30 G. Kokot, D. Piet, G. M. Whitesides, I. S. Aranson and A. Snezhko, *Scientific Reports*, 2015, **5**, 9528.
- 31 G. Kokot, A. Snezhko and I. S. Aranson, *Soft Matter*, 2013, **9**, 6757–6760.
- 32 A. Snezhko, I. S. Aranson and W.-K. Kwok, *Phys. Rev. Lett.*, 2005, **94**, 108002.
- 33 A. Snezhko, *J. Phys.-Condens. Mat.*, 2011, **23**, 153101.
- 34 K. J. Solis and J. E. Martin, *Soft Matter*, 2013, **9**, 9182–9188.
- 35 A. Snezhko, I. S. Aranson and W.-K. Kwok, *Phys. Rev. E*, 2006, **73**, 041306.
- 36 P. Tierno, T. M. Fischer, T. H. Johansen and F. Sagues, *Phys. Rev. Lett.*, 2008, **100**, 148304.
- 37 A. Snezhko, M. Belkin, I. S. Aranson and W.-K. Kwok, *Phys. Rev. Lett.*, 2009, **102**, 118103.
- 38 J. Yan, M. Bloom, S. C. Bae, E. Luijten and S. Granick, *Nature*, 2012, **491**, 578–582.
- 39 A. Snezhko and I. S. Aranson, *Nat. Mater.*, 2011, **10**, 698–703.
- 40 E. Ben-Naim and P. Krapivsky, *Physical Review E*, 2002, **66**, 011309.